Normal Conducting Steady-State Toroidal Magnet Systems for Ignited Tokamaks

K. Borrass, M. Söll

IPP 4/203 July 1981

MAX-PLANCK-INSTITUT FÜR PLASMAPHYSIK

8046 GARCHING BEI MÜNCHEN

MAX-PLANCK-INSTITUT FÜR PLASMAPHYSIK

GARCHING BEI MÜNCHEN

Normal Conducting Steady-State Toroidal Magnet Systems for Ignited Tokamaks

K. Borrass, M. Söll

IPP 4/203 July 1981

Die nachstehende Arbeit wurde im Rahmen des Vertrages zwischen dem Max-Planck-Institut für Plasmaphysik und der Europäischen Atomgemeinschaft über die Zusammenarbeit auf dem Gebiete der Plasmaphysik durchgeführt.

IPP 4/203

Normal Conducting Steady-State Toroidal Magnet Systems for Ignited Tokamaks

K. Borrass, M. Söll

July 1981

ABSTRACT

Normal conducting steady-state toroidal magnet systems are investigated, emphasis being placed on applications to large ignited next generation tokamaks.

The study is based on water-cooled tape wound D-coils. The data for the TF magnet systems are calculated in a consistent manner with a computer program including the plasma, shield, ohmic heating coil system and geometric requirements for blanket modules, beam ducts etc. An optimisation procedure is used to find those TF coil systems which minimize cost-relevant quantities.

The main results are that normal conducting TF coil systems of ignited next-generation tokamaks (following JET, TFTR etc.) can be operated in a stationary mode and fed from the grid. Cost for electricity is a relatively small portion of the investment cost even in the case of long integral burn times ($>10^7$s).

1. INTRODUCTION

Within future tokamak development a certain fixed point is given by systems of the DEMO-INTOR type in that they require an ignited, relatively long burning plasma, superconducting toroidal field coils and a breeding blanket or blanket modules. Each of these goals requires a big step beyond the present status. Coupling all these options in a single experiment following JET or TFTR would constitute a major risk to achieving these aims.

Apart from a trivial time sequence procedure, decoupling of the risks could be achieved by making use of normal conducting TF coil systems for ignited plasmas and developing superconducting TF coils and ignited plasmas in separate devices. Such a procedure has already been proposed in "European Long-term Planning", in which emphasis is placed on time schedule requirements.[1]

In this study tape-wound, water-cooled D-coils with low mechanical stresses are considered with a view to application in ignited tokamaks. Such coils have been successfully manufactured for the JET device with specifications close to those of next-generation tokamaks. Apart from the greater experience in manufacturing and operating large, normal conducting TF magnets further advantages over superconducting magnets are:

- simpler mechanical structure of the winding and simpler cooling
- smaller radiation shielding
- immunity to rapid magnetic field variations (disruptions)
- easier (radial and lateral) support of the winding
- easier dismantling (no cryostats)
- simpler detection and discharge systems.

The main drawback of normal conducting TF coils is the high resistive losses. Furthermore, since next-generation tokamaks should operate in the long-pulsed mode, steady-state operation, and hence steady-state cooling, is required. There is an obvious trade-off between resistive losses and cooling requirements on the one hand and stored magnetic energy and coil thickness on the other. This paper is to clarify quantitatively whether next-generation ignited tokamaks with resistive steady-state TF coils with acceptable size and resistive losses can be built. For this purpose a model that allows for the self-consistent layout of such systems is developed. The solutions are optimized with respect to cost-relevant figures of merit and take into account all relevant technical and geometrical constraints.

Though this paper is devoted to next-generation tokamaks it is pointed out that the model also applies to current, non-ignited experiments as well as to hybrid and pure fusion reactors.

Other concepts for steady-state normal conducting TF coils were studied in Refs. [2, 3, 4], the underlying philosophy being different in part. In our study emphasis was placed on risk minimization, and consequently medium-field, low-stress coils, the fabrication of which is standard, were considered. For easier dismantling the analysis of Refs. [2, 3] is based on rectangular TF coils assembled from copper plates. In contradiction to this and our study, Ref. [4] deals with compact tokamaks with Bitter-type TF systems exposed to high mechanical stresses.

2. MODEL DESCRIPTION

2.1 Geometry

The analysis is based on tape-wound D-coil systems as shown in Fig. 1. The plasma is centred at R_o (plasma major radius). The elongated plasma cross-section is characterized by the minor radius a and the plasma elongation s. The plasma is surrounded by a scrape-off layer of thickness l, a vessel of thickness u and a shielding of thickness D.

The D-coil is characterized by the minimum and maximum distances of the centre line from the torus axis, R_1 and R_2 respectively, and by the coil thickness Δ. The coils are tapered in the inner coil region in order to make optimum use of the limited area in this region. Each coil is subdivided into m pancakes, the typical case where m = 2 being shown in Fig. 1. The toroidal field coils are supported by the central support cylinder of thickness t_1 (see Fig. 2). The ohmic heating coil has a thickness Δt and a radius R_{OH} as shown in Fig. 2.

There are further important geometrical parameters, namely g, ΔR and d, of which g and ΔR are visualized in Fig. 1. The parameter g characterizes the free space available for the installation of, for instance, a poloidal divertor, while ΔR characterizes the space available for the installation of, for instance, blanket

modules. The parameter d is the free space between two coils in the equatorial plane and gives the space for beam ducts etc. Depending on the specific system under consideration, lower limits g^m, ΔR^m and d^m exist for the quantities g, ΔR and d.

2.2 Basic Equations

The following set of equations forms the central part of the model. They can obviously be evaluated in the given order, once the first two groups of parameters of Table I are given. The relations are only commented on if necessary. All units are MKSA units if not otherwise stated.

2.2.1 Geometric Relations

$$a^* = a\sqrt{s} \tag{1}$$

(radius of an equivalent circular plasma)

$$R_o = a\,A \tag{2}$$

(major radius)

$$V = 2\pi^2 a^{*2} R_o \tag{3}$$

(plasma volume)

$$R_1 = R_o - a - l - u - D - \Delta/2 \qquad (4)$$

(see Fig. 1)

$$h_o = s\,a + l + u + D + g^m \qquad (5)$$

(see Fig. 1)

h_o is the minimum value of h, such that $g \geq g^m$.

$$R_{2O} = R_o + a + l + u + D + \Delta/2 + \Delta R^m \qquad (6)$$

R_{2O} is the minimum value of R_2 such that $\Delta R \geq \Delta R^m$.

$$R'_{2O} = R_1 + \frac{(d^m+2D)N}{2\pi} + \Delta \qquad (7)$$

R'_{2O} is the minimum value of R_2 such that $d \geq d^m$.

$$R''_{2O} = R_1((1.257\times10^2+29.91(h_o+\Delta/2)/R_1)^{0.5}-10.10) \qquad (8)$$

R''_{2O} is the minimum value of R_2 such that $g \geq g^m$.
See also eq. (10).

$$R_2 = \max\{R_{2O}, R'_{2O}, R''_{2O}\} \qquad (9)$$

R_2 is the minimum value such that the constraints $g \geq g^m$, $\Delta R \geq \Delta R^m$ and $d \geq d^m$ are met.

$$h = R_1(3.344\times10^{-2}(R_2/R_1)^2+6.757\times10^{-1}\,R_2/R_1-0.7891)-\Delta/2 \qquad (10)$$

This is a polynomial fit of an analytic expression given in Ref. (10). The same relation was used in eq. (8).

$$g = h - s\,a - l - u - D \qquad (11)$$

(see Fig. 1).

$$d = \frac{2\pi\ (R_2 - R_1 - \Delta)}{N} - 2\ D \qquad (12)$$

(coil distance in the equatorial plane)

$$\Delta R = R_2 - R_{2O} + \Delta R^m \qquad (13)$$

(see Fig. 1)

Equations (11), (12), (13) give the actual values of g, d and ΔR.

$$R = R_o + a \qquad (14)$$

$$\varepsilon[\%] = 5.4\times10^2\ \frac{R\ R_1 (R_2/R_1-1)^{1.5} (R_2-R_1)}{N^4 ((R_2-R)^2 + (\pi R_2/2N)^2)^{1.5}}$$

$$\frac{\pi^3+4\pi\ N^2(1-R/R_2)R/R_2}{\pi^2+4\ N^2(1-R/R_2)^2} \qquad (15)$$

(field ripple at $R^{(5)}$)

2.2.2 Plasma-Related Quantities

$$\bar{\beta}_t = 0.12\ s/A \qquad (16)$$

$\bar{\beta}_t$ is the volume averaged toroidal beta. This scaling of $\bar{\beta}_t$ is widely accepted for not too strong elongation ($s \lesssim 2.0$) and not too low aspect ratios ($A \gtrsim 2.5$).

$$B_t^o = \left(\frac{(1-C_s)\ C}{\bar{\beta}_t^2\ a^{*2}}\right)^{1/4} \qquad (17)$$

Equation (17) is the ignition condition for a plasma which is dominated by anomalous electron heat conduction of the ALCATOR-type. ALCATOR-type losses typically dominate neoclassical ion heat conduction, except for rather high densities. Bremsstrahlung losses can typically be neglected, provided that the working point of the system is not located too far into the ignition regime. In this approximation the ignition condition simplifies to $Q_\alpha - Q_{loss} \geq 0$, where Q_α is the α-heating term and Q_{loss} the transport loss term in the energy balance. With $Q_\alpha \sim \bar{\beta}_t^2 B_t^{o\,4} f(T)$ and $Q_{loss} \sim T/a^{*2}$ it then follows that ignition requires that $\bar{\beta}_t^2 B_t^{o\,4} a^{*2} \geq C$, where C can be taken as constant, if one assumes that the working temperature is close to the minimum of $T/f(T)$. The constant C measures the safety of ignition, a value of $C \simeq 1.8$ corresponding to marginal ignition. Other transport models can easily be implemented. Confinement to ALCATOR scaling was made in this study to allow comparison with systems such as JET and INTOR, which have been studied in detail on the basis of this model.

Driven systems can be treated by taking $C_s > 0$. Considering a system with the same working temperature as an ignited one with margin C, but driven by auxiliary heating with power density Q_h, one has $(Q_\alpha + Q_h)/Q_{loss} = C$. Setting $Q_h/Q_{loss} = C_s$ it then follows that $\bar{\beta}_t^2 B_t^{o} a^{*2} = (1 - C_s)\, C$, which is equivalent to eq. (17).

$$p_f\ [\mathrm{MW\ m^{-3}}] = 2.0\ \bar{\beta}_t^2\ B_t^{o\ 4} \tag{18}$$

Using this approximation for the fusion power density p_f, it is assumed that T lies in a range where $\langle\sigma v\rangle \sim T^2$ is valid for the reaction rate. This is typically compatible with the assumption about T in the derivation of eq. (17). The factor of proportionality in eq. (18) depends on both the T and n profiles. The value of 2.0 can be achieved by moderately peaked T and nearly flat n profiles. Even higher values could be obtained if the n-profiles were more peaked in large tokamaks than predicted by current transport codes.

$$P_f[\mathrm{MW}] = V\ p_f \tag{19}$$

(fusion power)

$$P_\alpha[\mathrm{MW}] = 0.2\ P_f \tag{20}$$

(α-power)

$$N_n[\mathrm{MW\ m^{-2}}] = 0.4\ p_f\ \frac{a^{*2}}{a^*(1+s)/(2s^{1/2})+1} \tag{21}$$

(mean neutron wall load)

$$P_h[\mathrm{MW}] = \frac{C_s\ P_\alpha}{(1-C_s)\,\eta_h} \tag{22}$$

(heating power in a driven system)

$$W_{int}\ [MW\ y\ m^{-2}] = \frac{N_n\ \tau_{tot}}{3.154 \times 10^7} \qquad (23)$$

(integral wall load)

$$\tau_{iso}\ [s] = \frac{1.13 \times 10^5}{N_n}\ e^{15.35\ D} \qquad (24)$$

τ_{iso} is the lifetime of the insulation, which determines the lifetime of normal conducting coils. A maximum allowable dose rate of 5×10^9 rad and the equivalence 1 rad = 10^{13} n/m^2 was used.[6, 7]

$$T_c\ [g] = 1.779 \times 10^{-6}\ P_f\ \tau_{tot} \qquad (25)$$

(total tritium consumption)

2.2.3 Toroidal Field System

$$B_m = \frac{B_t^o\ R_o}{R_1 + \Delta/2} \qquad (26)$$

(magnetic field at $R_1 + \Delta/2$)

$$K = \frac{1}{2}\ \ln\left(\frac{R_2}{R_1}\right) \qquad (27)$$

(coil parameter [8])

$$\sigma = \frac{K}{2\mu_o}\ \frac{B_m^2\ (R_1 + \Delta/2)^2}{R_1\ F\ \Delta} \qquad (28)$$

σ is the mechanical tensile stress for D-coils. The study anticipates that the TF coils are wound with conductors fabricated from microalloyed copper (oxygen-free

copper with 0.1 % silver). The yield limit of this conductor used for the JET toroidal coil system [9] is in the range of 200 - 250 MPa.

$$\sigma_D = \frac{B_m^2 (R_1 + \Delta/2)^2}{2\mu_o \; R_1^2} \tag{29}$$

(pressure on the support cylinder due to the centripetal force)

$$\rho = 2 \times 10^{-8} \tag{30}$$

(specific resistivity of copper at 80° C)

$$P_{ohm}[MW] = \frac{4\pi^2 \; 10^{-6}}{\mu_o^2} \; \frac{\rho \; K \; e^K (R_1 + \Delta/2)}{F \; \Delta} \; B_m^2$$

$$((R_1 + \Delta/2) \; I_1(K) + R_1 \; I_o(K)) \tag{31}$$

P_{ohm} denotes the resistive losses, and I_o and I_1 are the modified Bessel functions of zero and first order respectively.

$$V_{Cu} = 4 \; \pi^2 \; \Delta \; K \; e^K \; R_1 \; F \tag{32}$$

$$(R_1 \; I_1(K) + (R_1 + \Delta/2) \; I_o(K))$$

(volume of copper)

$$\rho_{Cu} = 8.9 \times 10^3 \tag{33}$$

(density of copper)

$$M_{Cu} = \rho_{Cu} V_{Cu} \tag{34}$$

(mass of copper)

$$E_m[MJ] = \frac{2\pi^2 10^{-6}}{\mu_o} K e^K B_m^2 R_1 (R_1+\Delta/2)^2$$

$$(K I_o(K) + (K - 1) I_1(K)) \tag{35}$$

(stored magnetic energy)

$$j = \frac{B_m (R_1+\Delta/2)}{\mu_o \Delta F R_1} \tag{36}$$

(peak current density in TF coils)

Equations (31) and (32) can easily be derived once the average length of a conductor per turn is known (see eq. (38)). Equation (35) is taken from Ref.[10]. Equation (36) follows from Ampere's law.

2.2.4 Cooling

$$P_o [MW] = \frac{P_{ohm}}{m N} \tag{37}$$

(ohmic losses per pancake)

$$l_o = 2 \pi R_1 K e^K (I_o(K) + I_1(K)) \tag{38}$$

l_o is the average length of a conductor per turn [10].

$$L = n_L l_o \tag{39}$$

(length of a conductor per pancake)

$$Q_L = 2.389 \times 10^{-1} \frac{P_o}{n_s \Delta T} \quad (40)$$

(water flow per cooling channel)

$$Q = Q_L \, m \, n_s \, N \quad (41)$$

(total water flow)

$$d = \left(\frac{8 \, (F_I - F) \Delta \, R_1}{m \, n_L \, N \, n_c}\right)^{1/2} \quad (42)$$

(hydraulic diameter of cooling channel)

$$\Delta P = 2.44 \times 10^{-4} \frac{Q_L^{\,2} \, L \, n_c}{n_s \, d^5} \quad (43)$$

(pressure drop per cooling channel)

$$v = \frac{4 \, Q_L}{\pi \, d^2} \quad (44)$$

(velocity of water)

$$T_b \, [C^o] = T_o + \Delta T/2 \quad (45)$$

(mean temperature of water)

$$\dot{q} \, [W \, m^{-2}] = \frac{10^6 \, P_o}{\pi \, d \, L \, n_c} \quad (46)$$

(heat flux)

$$\eta \, [W \, m^{-2} \, C^{o \, -1}] = 1.42 \times 10^3 \, (1 + 1.5 \times 10^{-2} \, T_b) \, \frac{v^{0.8}}{d^{0.2}} \quad (47)$$

(heat transfer coefficient)

$$\Delta T_w \, [C^o] = \dot{q}/\eta \quad (48)$$

(temperature difference between conductor surface and coolant)

$$T_{max}\ [C^{o}] = T_{o} + \Delta T + \Delta T_{w} \qquad (49)$$

(maximum coil temperature)

$$L_{pump}\ [MW] = 7.854 \times 10^{-2}\ \Delta P\ d^{2} v\ m\ N\ n_{s} \qquad (50)$$

(total pumping power)

The above treatment of the cooling problem is based on Ref.[11].

2.2.5 Core Constraint

To take into account the core constraint, the coupling of the OH coil to the plasma ring has to be considered. Figure 2 shows the OH coil arrangement and the notations used.

$$t_{1} = 0.1 \qquad (51)$$

t_1 is the thickness of the central support cylinder. A fixed value is used throughout.

$$R^{o}_{OH} = R_{1} - \Delta/2 - t_{1} \qquad (52)$$

(maximum OH coil radius; see Fig. 2)

$$\Delta t = 0.58\ R^{o}_{OH} \qquad (53)$$

Δt is the thickness of the OH coil. The factor of 0.58 is explained below.

$$R_{OH} = R_{OH}^{o} - 0.5\ \Delta t \qquad (54)$$

(OH coil radius)

$$I_p = \frac{2\pi}{\mu_o} \frac{B_t^o\ a^{*2}}{q(a) R_o} \frac{1 + s^2}{2\ s} \qquad (55)$$

(plasma current in case of an elongated plasma [9])

$$l_i = 1 \qquad (56)$$

(internal plasma inductance per unit length in units of $\mu_o\ R_o/2$)

$$L_p = \mu_o\ R_o\ (\ln(8R_o/a^*) - 2 + l_i/2) \qquad (57)$$

(plasma inductance)

$$f = 2 \qquad (58)$$

(enhancement factor for poloidal flux; see note below)

$$B_{OH} = \frac{f\ I_p\ L_p}{2\ \pi\ R_{OH}^2} \qquad (59)$$

B_{OH} is the field at the OH coil. Equation (59) is the approximate transformer equation for the OH coil - plasma ring system. Resistive losses are estimated by taking $f > 1$. Equation (59) is pessimistic in that contributions by the vertical field are ignored.

Taking this into account, a value of f = 2 seems sufficient to compensate for the resistive losses during start-up and a burn of approximately one L_p/R_p-time length.

$$j_{OH} = \frac{B_{OH}}{\mu_o \Delta t} \qquad (60)$$

(OH coil current density)

$$\sigma_{OH} = \frac{B_{OH}^2 R_{OH}}{2 \mu_o \Delta t} \qquad (61)$$

(OH coil tensile stress)

Both quantities j_{OH} and σ_{OH} are subject to upper limits. One can choose Δt such that for fixed R_{OH}^o either j_{OH} or σ_{OH} has a minimum value. j_{OH} takes its minimum for $\Delta t = 2/3\ R_{OH}^o$, while σ_{OH} is minimal if $\Delta t = 0.5\ R_{OH}^o$. Since both minima are relatively weak, the mean value $\Delta t = 0.58\ R_{OH}^o$ was taken in eq. (53).

2.2.6 Figure of Merit

A rough cost estimation is used as a figure of merit for the optimization procedure to be described below.

$$\emptyset_1\ [DM] = C_{el} \frac{\tau_{tot}\ (P_{ohm} + P_h)}{3.6} \qquad (62)$$

(cost of electricity; see eqs. (22) and (31))

$$\emptyset_2 \text{ [DM]} = C_{magn} E_m \qquad (63)$$

(investment cost)

$$\emptyset_3 \text{ [DM]} = C_T T_c \qquad (64)$$

(cost of tritium; see eq. (25))

$$\emptyset \text{ [DM]} = \emptyset_1 + \emptyset_2 + \emptyset_3 \qquad (65)$$

$\emptyset_1$ gives the cost of the consumed electric energy. $\emptyset_3$ is the cost of the burned tritium. Both the cost of installation and the cost for the tritium inventory can be roughly included by taking enhanced values for C_{el} and C_T. Equation (63) estimates the investment costs by the stored magnetic energy.

2.3 Constraints and Optimization

In practice, several of the quantities resulting from the equations of the preceding section underly constraints, which are of a geometrical nature or stem from materials or technical limitations. The following constraints are involved in our model:

$$g \geq g^m \tag{66}$$

$$\Delta R \geq \Delta R^m \tag{67}$$

$$d \geq d^m \tag{68}$$

Here g^m, ΔR^m and d^m have the meaning outlined above.

$$\varepsilon \leq \varepsilon^m \tag{69}$$

$$\sigma \leq \sigma^m \tag{70}$$

ε^m is the maximum field ripple, while σ^m gives the maximum tensile stress in the TF coils.

The core constraint is taken into account by the conditions

$$\sigma_{OH} \leq \sigma_{OH}^m \tag{71}$$

and

$$j_{OH} \leq j_{OH}^m \,, \tag{72}$$

where σ_{OH}^m is the maximum tensile stress in the OH coils, and j_{OH}^m the maximum OH coil current density.

The total burn time should not exceed the insulation lifetime, so that

$$\tau_{iso} \geq \tau_{tot} \tag{73}$$

must hold. This condition essentially determines the shielding thickness if τ_{tot} is prescribed.

In certain cases (material tests, blanket test modules) the wall load N_n and the integral wall load W_{int} are limited to below:

$$N_n \geq N_n^m \,, \tag{74}$$

$$W_{int} \geq W_{int}^m \,. \tag{75}$$

It is pointed out that all the quantities g, ΔR, d, ε, σ, σ_{OH}, j_{OH}, τ_{iso}, N_n, W_{int} result, when evaluating the set of equations given in the preceding section.

In general, the constraints do not determine a unique solution of the basic equations. This means that generally for a wide range of input parameters a, A, s, ... the basic equations can be solved while simultaneously meeting the constraints according to eqs. (66) to (75). A unique solution is found by determining that combination of input parameters that minimizes the figure of merit Φ as given by eq. (65).

The optimization procedure runs as follows. The input parameters of the second group in Table I are kept fixed throughout. They are either not subject to manipulations (such as q(a)) and/or only have a weak influence on relevant quantities (l, T_o, ΔT etc.). Intervals $[a_1\ a_2]$, $[A_1\ A_2]$, ..., $[C_1\ C_2]$ are given for the input parameters of the first group. The six-dimensional space spanned by these intervals is covered with a six-dimensional, equidistant grid. For each grid point the computer runs through eqs. (1) to (65) of Sec. 2.2. Whenever the resulting $\emptyset$ value is larger than the stored one or if any of the constraints is violated, the results for this grid point are ignored and the computation is repeated for the next point. In the opposite case the results for this grid point, including $\emptyset$ and the values for a, A, ..., C, are stored.
After the computation has been performed for all grid points, the stored one is that yielding a solution with minimum $\emptyset$. Around this point a new grid of smaller size is defined and the whole procedure is repeated. This procedure is iterated to the desired accuracy.

Owing to its discrete nature the coil number N requires a distinct treatment. At first the optimum solutions are determined as described above, N being kept fixed. After repetition for all N with $N_1 \leq 2\ N \leq N_2$, where N_1, N_2 are input parameters, the one that yields a minimum value for $\emptyset$ is selected and taken as final solution.

The number of grid points, the number of subsequent grids and the reduction factor for the grid size can be prescribed as input parameters.

The number of grid points, and hence the computation time, strongly increases with the grid dimension. In order not to exceed the number of six variables, R_2 was chosen according to eq. (9). This choice affords a trivial optimization since any reasonable figure of merit is minimized by choosing R_2 in this way.

If the input intervals $[a_1\ a_2]$, $[A_1\ A_2]$, ..., $[C_1\ C_2]$, $[N_1\ N_2]$ are appropriately chosen, the resulting values for a, A, ., C, N should not coincide with either of the boundaries. This, however, may be impossible if the range of some variable is limited by physical or technical constraints. The elongation s, for instance, generally tends to take the maximum value s_2. The upper boundary s_2 of the input interval thus practically constitutes an additional constraint. A similar situation prevails for the ignition factor C, which generally takes its minimum value C_1, except when N_n^m is sufficiently high. In such cases the respective variable can be explicitly prescribed. The grid dimension, and hence the computation time, is then considerably reduced.

The optimization procedure described yields sufficient accuracy with modest computation time. A typical run with maximum grid dimension yielding an accuracy of a few p.p.th. requires less than 60 s on a CRAY I. A significant advantage of the method lies in the simplicity with which constraints can be taken into account.

3. RESULTS

The following three systems are discussed in greater detail and taken as reference points for subsequent parameter studies:

I A pure physics experiment to study ignited, long burning D-T plasmas.

II An ignited, long burning tokamak which has a neutron wall load and integral neutron flux that allows material tests.

III A system with the same specifications as II but with additional space for the implementation of blanket test modules.

The complete set of input parameters for these three systems is given in Table II. In all three cases f = 2 was set in eq. (59), allowing burn times of up to roughly one plasma L_p/R_p-time.

For system I the required integral burn time would follow from the envisaged experimental programme and hence is explicitly given. For systems II and III τ_{tot} is self-consistently determined from W_{int} and N_n.

The complete set of output data is listed in Table III. In all three cases s and C take the boundary values, s_2 and C_1 respectively. With respect to the core constraint eq. (72) is typically more restrictive than eq. (71). As expected, D always adjusts so that $\tau_{iso} = \tau_{tot}$. σ is always close to σ^m. In cases I and II the coil number N is mainly determined by the conditions $d \geq d^m$ and $\varepsilon \leq \varepsilon^m$, resulting in a value $\Delta R \geq 0$. In system III the condition $\Delta R \geq \Delta R^m$ is more restrictive, and solutions exist with different N but identical $\emptyset$ that satisfy both eq. (68) and eq. (69). Among these the solution with minimum N was selected, yielding maximum d.

Several important conclusions can be drawn from Table III:

- Stationary cooling can be achieved without difficulties in all three cases. For typical values of F, F_I, n_L, n_s, T_o and ΔT all critical parameters such as T_{max}, ΔP are found to be on the safe side. Furthermore, the flow velocity is sufficiently low to avoid cavitation.

- The resistive losses do not exceed 500 MW. The systems could thus be fed from the grid in principle.

- For all three systems both the cost of electricity and the cost of tritium are at least one order of magnitude smaller than the investment costs. Hence, though the estimation of the investment costs is very rough, all three systems would probably be dominated by the investment costs.

- There is a relatively big jump in stored magnetic energy between systems I and II. On the other hand, there is only a modest increase in stored energy when going from system II to III. Systems of type I (pure physics experiment) or type III (physics, materials testing, blanket test modules) are natural candidates for next-generation tokamaks with normal conducting TF coils.

The solutions of the model are largely determined by the constraints. In Fig. 3 the sensitivity of Ø to variations of the most relevant constraints and the integral burn time τ_{tot} is visualized. System I was taken as reference system. The strong dependence on s is striking. It explains the general tendency of the systems to take the maximum possible value for s. Considering the dependence on τ_{tot} and d^m, one recognizes that there is a continuous transition from system I to those of type II or III.

In our examples, since the cost of electricity does not significantly contribute to $\emptyset$, Δ reduces until σ reaches its limit value. There may be additional constraints, such as political ones, that make it desirable to reduce the resistive losses by increasing the coil thickness, despite the resulting increase in stored energy. Figure 4 shows how $\emptyset$ and P_{ohm} vary if Δ deviates from its optimum value. System I was taken as reference case. With increasing Δ the relative gain in P_{ohm} equals the relative loss in $\emptyset$. A drastic reduction of the resistive losses by increasing the coil thickness would thus probably lead to an unacceptably high stored energy.

In devices the main purpose of which is neutron production it might be advantageous to operate in the non-ignited mode and drive the system by additional heating. This can be crudely simulated by taking $C_s > 0$. Figure 5 shows the variation of $\emptyset$ with C_s. System III was taken as reference system. The discontinuities in Fig. 5 are related to jumps in the coil number N. Additional heating only has a weak effect on $\emptyset$, the reason being that C increases with increasing C_s so that $C_{eff} = C\ (1 - C_s)$ remains nearly constant. The increase of C above its lower limit is required to keep B_t^o and hence N_n sufficiently high to meet the condition $N_n \geq N_n^m$.

4. CONCLUSION

Water-cooled, steady-state resistive TF coil systems have been studied for application in next-generation ignited tokamaks. D-shaped, tape-wound coils were selected to minimize risk. Tried fabrication techniques are available for such coils, and a TF system with specifications close to those of next-generation tokamaks has been successfully manufactured for the JET device.

The feasibility of such systems was studied within the framework of a self-consistent layout model. Besides describing the main system components (plasma, TF coils, OH system, cooling),this model takes into account all relevant technical and geometrical constraints. The resulting data sets describe systems which, in addition, are optimized with respect to cost relevant quantities.

For a wide range of specifications (pure physics experiment, materials testing and blanket testing facilities) our investigation yields the following main results:

- The TF coils can be operated in steady-state without difficulties (low pressure drop in the coolant channel, low flow velocities).

- The resistive losses are sufficiently low to feed the TF coil system from the grid.

- The cost of electricity is relatively small compared with investment costs.

- The coils can be operated at low operational load (low mechanical stresses, tensile stresses below 80 MPa).

The main purpose of this paper is to assess the basic feasibility of normal conducting TF coil systems for long-pulsed, ignited tokamaks. When comparing such systems with, for instance, superconducting TF coil systems, complete lines of development towards a demonstration plant have ultimately to be compared from a cost-risk point of view. As a contribution to such an undertaking, similar calculations for superconducting TF coil systems are under preparation[12].

Acknowledgement

The authors wish to thank experts from BBC Mannheim and Zürich for their contributions to a discussion meeting on the manufacture of large toroidal magnet systems.
Valuable information contributed by K.H. Schmitter and J. Raeder and the programming work by H. Gorenflo are gratefully acknowledged.

REFERENCES

1. B. Brandt, C. Casini, J. Varras, F. Engelmann, G. Grieger, H. Persson, R. Verbeek, Long Term Planning towards a Demonstration Fusion Reactor, EUR FU XII/708/77/LTP50

2. J. Kalnavarns, D.L. Jassby, Steady-state resistive toroidal-field coils for tokamak reactors, Proc. 8th Symp. on Eng. Probl. of Fusion Research (San Francisco, CA, 1979) pp. 148-153

3. J. Kalnavarns, D.L. Jassby, Resistive Toroidal-Field Coils for Tokamak Reactors, PPPL-1685, Plasma Physics Laboratory, Princeton University (November 1980)

4. L. Bromberg, D.R. Cohn, Use of high performance resistive magnet tokamaks as advanced test reactors and fissile fuel breeders, PFC/RR-81-16, Plasma Fusion Center, M.I.T. (April 1981)

5. M. Söll, An analytical approach for calculating the magnetic field ripple of toroidal D-coil magnet systems, Interner Bericht No. 24, Max-Planck-Institut für Plasmaphysik Garching, Projekt Systemstudien (June 1979)

6. A.A. Koch, J.C. Rauch, K.-J. Greve, Insulation systems and winding technique for large coils in fusion experiments, 6th International Conf. on Magnet Technology (Bratislava, 1977), pp. 134-141

7. H. Brockmann, H. Krause, U. Ohlig, 1D Radiation Analysis for the Fusion Ignition Experiment ZEPHYR, IPP 1/173, Max-Planck-Institut für Plasmaphysik Garching (November 1979)

8. J. File, R.G. Mills, G.V. Sheffield, Large Superconducting Magnet Designs for Fusion Reactors, MATT-848, Plasma Physics Laboratory, Princeton University (June 1971)

9. The JET project - design proposal, EUR-JET-R5 (September 1975)

10. J. Raeder, Some analytical results for toroidal magnetic field coils with elongated minor cross-sections, IPP 4/141, Max-Planck-Institut für Plasmaphysik Garching (September 1976)

11. D.B. Montgomery, Solenoid Magnet Design, Wiley-Interscience (1969)

12. K. Borrass, M. Söll, paper to be presented at the 9th Symposium on Engineering Problems of Fusion Research (Chicago 1981).

INPUT PARAMETERS

a	(m)	plasma minor radius	
A		aspect ratio	GROUP I
s		elongation	selfconsistently
D	(m)	shielding thickness	determined
Δ	(m)	coil thickness	
C		ignition factor	
$q(a)$		plasma safety factor at boundary	
l	(m)	scrape-off layer thickness	
u	(m)	vessel thickness	
F		total filling factor	
F_I		isolation filling factor	
n_L		layers per pancake	
m		number of pancakes	GROUP II
n_c		number of cooling channels per layer	fixed
n_s		number of cooling channels per pancake	
T_o	(C^o)	coolant inlet temperature	
ΔT	(C^o)	coolant temperature rise	
τ_{tot}	(s)	integral burn time	
C_{mag}	(DM MJ^{-1})	specific cost of stored magnetic energy	
C_{el}	(DM kWh^{-1})	specific cost of electric energy	
C_{trit}	(DM g^{-1})	specific tritium cost	
ϵ^m	(%)	maximum allowable field ripple	
s^m		maximum elongation	
σ^m	(MPa)	maximum tensile stress	
g^m	(m)	minimum value for g (see Fig. 1)	
d^m	(m)	minimum distance between two coils (equatorial plane)	GROUP III
σ^m_{OH}	(MPa)	maximum OH-trafo tensile stress	constraints
j^m_{OH}	(A m^{-2})	maximum OH-current density	
ΔR^m	(m)	minimum value for ΔR (see Fig. 1)	
N_n^m	(NW m^{-2})	minimum neutron wall load	
W_{int}	(MW y m^{-2})	minimum integral wall load	
ΔP^m	(at)	maximum pressure drop per channel	
C^m		minimum ignition factor	

Table I

Set of input parameters required for solution of the basic equations

INPUT

SYSTEM		I	II	III	
CONSTRAINTS					
ι^m	(%)	1	-	-	maximum allowable field ripple
s^m		1.5	-	-	maximum elongation
σ^m	(MPa)	80	-	-	maximum tensile stress
g^m	(m)	1.0	-	-	minimum value for g (see Fig. 1)
d^m	(m)	0.65	-	-	minimum distance between two coils (equatorial plane)
σ^m_{OH}	(MPa)	150	-	-	maximum OH-trafo tensile stress
j^m_{OH}	($A\ m^{-2}$)	$1.5 \cdot 10^7$	-	-	maximum OH-current density
ΔR^m	(m)	0	-	1	minimum value for ΔR (see Fig. 1)
N_n^m	($MW\ m^{-2}$)	0	1	-	minimum neutron wall load
W^m_{int}	($MW\ y\ m^{-2}$)	0	1	-	minimum integral wall load
Δp^m	(at)	5	-	-	maximum pressure drop per channel
C^m		2.5	-	-	minimum ignition factor
FIXED INPUT PARAMETERS					
q(a)		2.5	-	-	plasma safety factor at boundary
l	(m)	0.09	-	-	scrape-off layer thickness
u	(m)	0.1	-	-	vessel thickness
F		0.7	-	-	total filling factor
F_I		0.8	-	-	isolation filling factor
n_L		16	-	-	layers per pancake
m		2	-	-	number of pancakes
n_c		2	-	-	number of cooling channels per layer
n_s		32	-	-	number of cooling channels per pancake
T_o	(C^o)	20	-	-	coolant inlet temperature
ΔT	(C^o)	40	-	-	coolant temperature rize
τ_{tot}	(s)	$2 \cdot 10^6$	+	+	integral burn time
C_{mag}	($DM\ MJ^{-1}$)	$1.5 \cdot 10^6$	-	-	specific cost of stored magnetic energy
C_{el}	($DM\ KWh^{-1}$)	0.15	-	-	specific cost of electric energy
C_{trit}	($DM\ g^{-1}$)	$7 \cdot 10^3$	-	-	specific tritium cost

Table II

Complete list of input parameters for reference systems I, II and III. C_{mag} was estimated from the approximate cost of 2 x 10^9 DM for the extended JET version with $E_m \simeq 1.4$ GJ.

OUTPUT

SYSTEM		I	II	III	
GEOMETRY					
a	(m)	1.56	1.43	1.53	plasma minor radius
A		2.50	2.91	2.78	aspect ratio
s		1.5	1.5	1.5	elongation
D	(m)	0.19	0.37	0.37	radiation shield thickness
Δ	(m)	0.50	0.69	0.65	coil thickness
ΔR	(m)	0.70	0.88	1.0	see Fig. 1
R_1	(m)	1.71	1.83	1.84	see Fig. 1
R_2	(m)	6.78	7.37	7.65	see Fig. 1
d	(m)	0.65	0.65	0.74	distance between two coils (equatorial plane)
g	(m)	1.16	1.48	1.62	see Fig. 1
N		28	22	22	number of coils
PLASMA					
$\bar{\beta}_t$	(%)	7.20	6.18	6.46	average toroidal beta
ε	(%)	0.99	1.00	0.97	field ripple
B_t^o	(T)	3.39	3.83	3.62	toroidal field at axis
P_f	(MW)	385	411	419	total fusion power
C		2.5	2.5	2.5	ignition factor
N_n	($MW\ m^{-2}$)	0.98	1.07	1.00	neutron wall load
W_{int}	($MW\ y\ m^{-2}$)	6.22×10^{-2}	1.00	1.00	integral wall load
τ_{tot}	(s)	2×10^6	2.95×10^7	3.14×10^7	total burn time
TORUS SYSTEM					
B_m	(T)	6.74	7.32	7.10	maximum toroidal field
σ	(MPa)	80	80	80	tensile stress
P_{OHM}	(MW)	460	484	505	resistive coil losses
E_m	(GJ)	4.24	6.82	6.93	stored magnetic energy
M_{Cu}	(kg)	8.14×10^5	1.35×10^6	1.35×10^6	mass of copper
j	($A\ m^{-2}$)	1.76×10^7	1.44×10^7	1.46×10^7	peak current density
σ_D	(MPa)	23.8	30.1	27.8	pressure on the support cylinder
OH-TRAFO					
σ_{OH}	(MPa)	107	111	114	OH-trafo tensile stress
j_{OH}	($A\ m^{-2}$)	1.50×10^7	1.50×10^7	1.48×10^7	OH-trafo current density
COOLING SYSTEM					
T_{max}	(C^o)	70.4	72.9	72.0	maximum coil temperature
d_c	(m)	1.95×10^{-2}	2.67×10^{-2}	2.61×10^{-2}	hydraulic diameter of cooling channel
ΔP	(at)	4.40	1.81	2.35	pressure drop per channel
L_{pump}	(MW)	1.21	0.52	0.71	pumping power
Q	($m^3\ s^{-1}$)	2.75	2.89	3.01	total coolant volume flow
v	($m\ s^{-1}$)	5.11	3.65	4.00	coolant flow velocity
FIGURES OF MERIT					
$\emptyset_1$	(DM)	3.83×10^7	5.95×10^8	6.61×10^8	cost of electricity
$\emptyset_2$	(DM)	6.36×10^9	1.02×10^{10}	1.04×10^{10}	investment cost
$\emptyset_3$	(DM)	9.58×10^6	1.51×10^8	1.64×10^8	tritium cost
$\emptyset$	(DM)	6.40×10^9	1.10×10^{10}	1.12×10^{10}	total cost

Table III

Complete list of output data for reference systems I, II and III

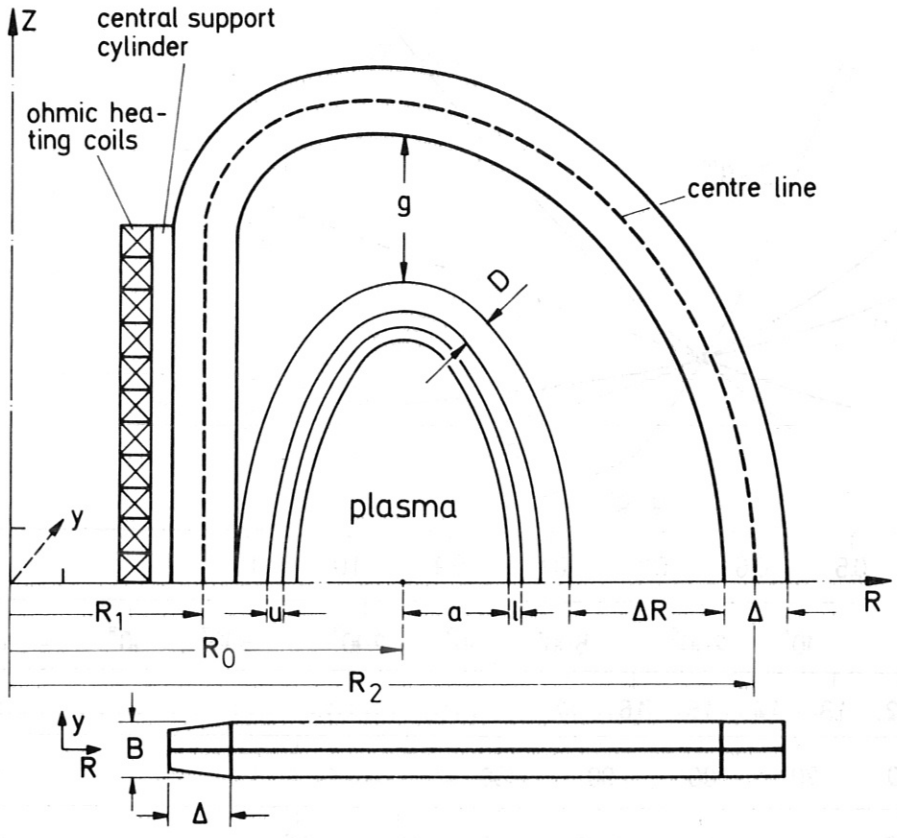

Fig. 1

Geometrical arrangement of main components

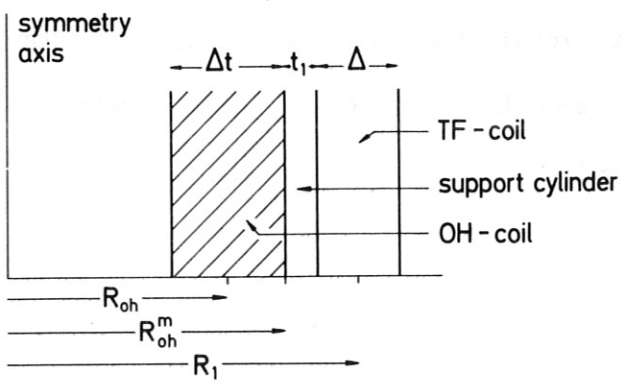

Fig. 2

Geometrical arrangement of the OH trafo and central support cylinder

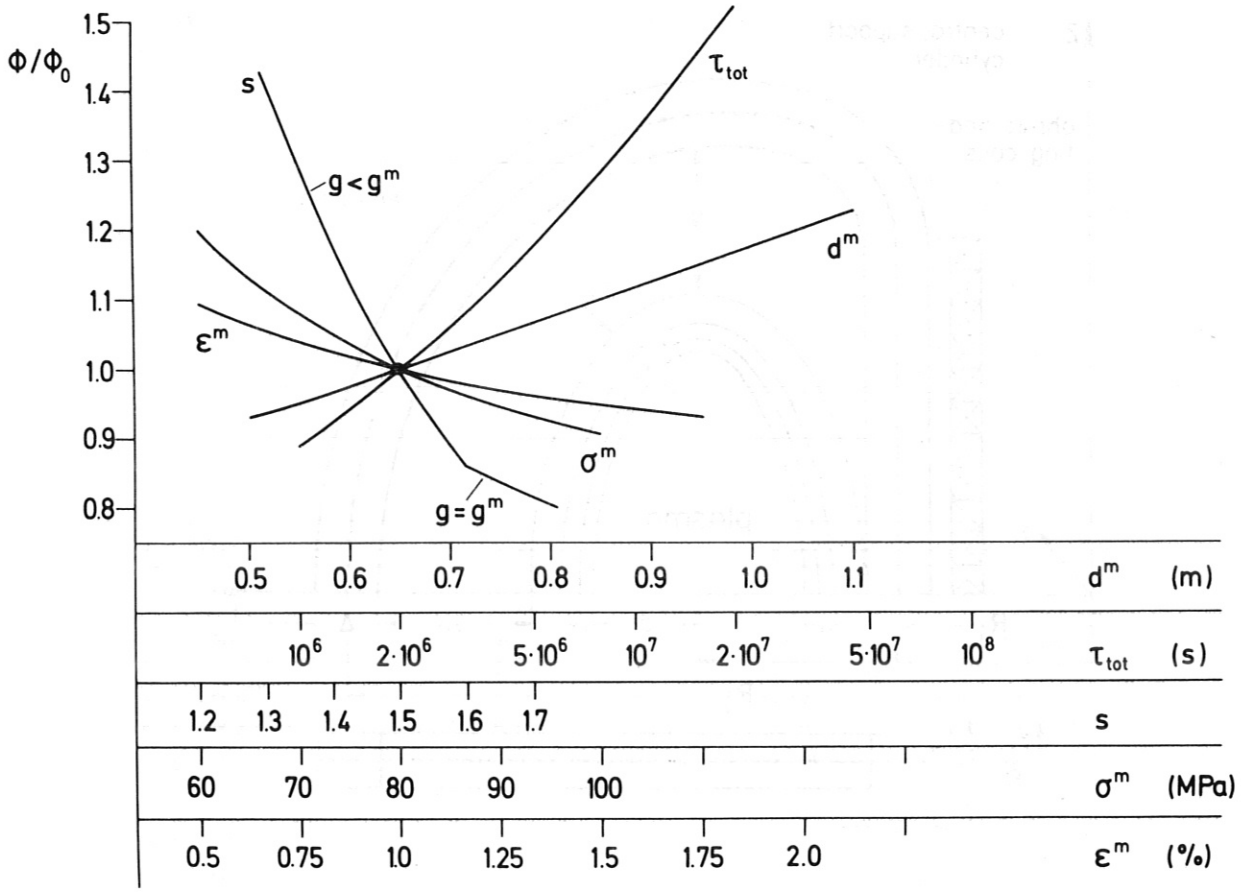

Fig. 3

Variation of the total cost (Ø) versus important constraints and the integral burn time (τ_{tot}). System I is taken as reference system

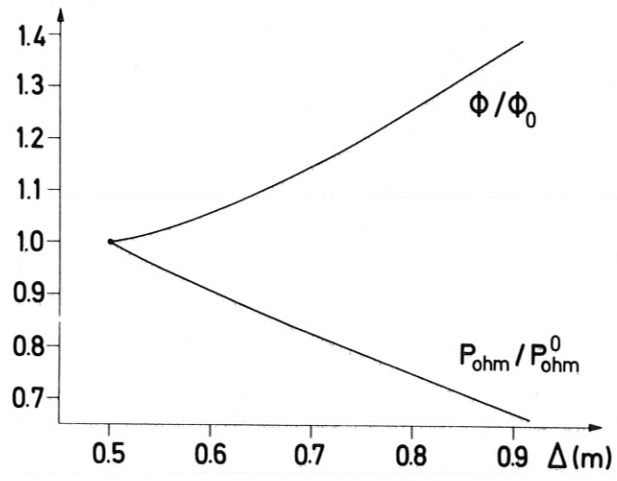

Fig. 4

Sensitivity of the total cost (Ø) and resistive losses (P_{ohm}) versus variations of the coil thickness (Δ). System I is taken as reference system

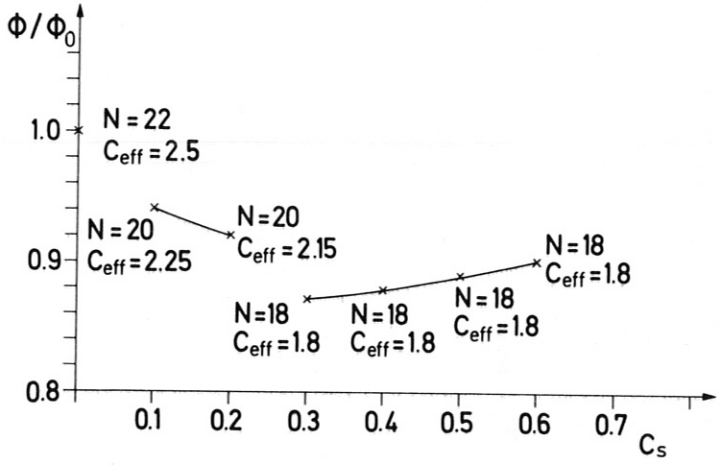

Fig. 5

Total cost variation in the case of a non-ignited, driven system. C_s measures the fraction of the plasma losses that is delivered by additional heating. System III is taken as reference system.